Journal of Marine Science and Technology (2023) 28:524–535
https://doi.org/10.1007/s00773-023-00938-5

ORIGINAL ARTICLE

# Parametric study of the oleophilic skimming process: CFD simulation using VOF model

**Eslam Reda Lotfy**[1]

Received: 27 May 2022 / Accepted: 31 March 2023 / Published online: 21 April 2023


## Abstract

Oleophilic skimming is a primary alternative when addressing oil spill accidents. However, the existing literature does not define accurately the optimum design and operating conditions of the oleophilic skimmer. In this research, an extensive CFD investigation was conducted on the performance of the drum skimmer. Seven parameters were tested, namely drum diameter, drum centre height, oil slick thickness, rotational speed, oil density, oil viscosity and oil surface tension. The simulations were performed by applying the volume of fluid technique using the OpenFOAM package. The two-dimensional numerical setup was tested for grid size, domain extension and time-step convergence, and the results were validated with experimental data from the literature. The skimmer performance was evaluated through the oil recovery rate and water ingestion rate. The study illustrated that the oleophilic drum skimmer best functions at rotational speed within 30–60 rpm, drum diameter within 200–300 mm, drum centre-height-to-diameter ratio within 0.3–0.4, oil slick thickness ≥ 15 mm and oil viscosity within 10–100 cSt.

**Keywords** CFD · Drum skimmer · Geometry · Oil properties · Rotational speed · Two-dimensional

## 1 Introduction

The persistent improvement of tanker safety standards and regulations have led to a great reduction in the amount of oil spilled in marine accidents [27]. However, human failure, equipment defects and unfavourable weather can never be excluded [9]. Major oil spills like the 2010 BP Deepwater Horizon oil spill in the Gulf of Mexico are still possible, and if happen can cause huge economic loss [22] and environmental damage that last for decades [14]. A wide set of oil spill removal approaches are available. Each approach is suitable for a particular case. Chemical dispersants and burning can cause deep environmental impacts. Moreover, chemical dispersion is not an adequate option in sub-zero temperature waters since bacterial degradation is completely suppressed [6, 38]. Physical skimming is the most environmentally friendly method, despite the high cost of construction and difficulty of application [45]. The oil recovery performance of oleophilic sorbent skimmers, e.g. rotating drums and conveyor belts, is negatively affected by wind and waves [11, 38]. Nevertheless, creative designs can overcome the environmental effects [3]. For a comparison between the characteristics of the different types of physical skimmers, the reader is referred to [3, 21]. In many instances, more than one strategy is deployed to remove the oil slack [38]. Apparently, research and development are carried on to improve the performance of oil removal techniques and facilitate their implementation.

Amongst all categories of physical skimmers, the oleophilic skimmers can recover oil in a spill accident with the least percentage of loss [25]. The performance of an oleophilic skimmer, i.e. the oil recovery rate, is a function of oil physical properties, oil slick thickness and height, and skimmer geometry, rotational speed and surface structure and material [8]. The oil recovery rate increases as the oil viscosity increases, slick thickness increases or rotational speed increases [31].

Many improvements were applied to the sorbent surface to upgrade its oil removal capacity. Broje and Keller [7] developed and tested a grooved pattern of the recovery surface of the drum skimmer and the matching scraper. The enhanced design proved to increase the efficiency to three

✉ Eslam Reda Lotfy
eslam.reda@alexu.edu.eg

[1] Department of Mechanical Engineering, Faculty of Engineering, Alexandria University, 21544 Alexandria, Egypt

times its value with the plain drum surface. The grooved drum skimmer works in a similar manner to the multiple disc skimmer and retains comparable amount of oil [36]. Broje and Keller [8] also compared the effect of three surface materials, namely aluminium, polyethylene and neoprene on the performance of oleophilic skimmers. They highlighted a pronounced role played by the surface material, essentially with thin slick thicknesses. The effect was attributed to the amount of water entrained by each material. Recently, Khalil et al [31] varnished the drum surface with a water-repelling nano-ceramics coating. They recorded a 21.5% increase in the oil recovery rate. Similarly, El-Gayar et al [16] compared steel, plastic and woven fabric as materials for the rotating disc skimmer and Algawai and Dawood [4] examined synthetic rubber, polyvinyl chloride and polypropylene as belt skimmer oleophilic materials. Sabbar et al [41] introduced a drum of fibreglass structure and four-layer painting of polyester resin material. Khalil et al [33] checked whether the pyramid-shaped surface roughness can improve the performance of the belt skimmer. It can be concluded that the smoother the sorbent surface is, the more oil is collected by the skimmer. Ultimately, an ideal zero-roughness surface would achieve the maximum possible oil recovery rate.

Computational Fluid Dynamics (CFD), although being the most powerful flow simulation tool, was seldom employed to model the oil removal problem. Abu-Amro and co-authors [2, 10, 12, 13] simulated the working principle of an innovative system for oil skimming vessels. Also, the hydrodynamics of the vacuum skimmer was simulated by Ni et al [39]. The operation of an oleophilic skimmer can be approximated by a simple mathematical model [20]. Nevertheless, the model overrides many details including the fact that the oil layer adheres to the rotating skimmer before dipping in water not after leaving it [31]. A rigorous simulation framework of the case is inevitable since experimenting the skimming process under realistic conditions is not available for most researchers. For instance, a small test tank exaggerates the amount of oil collected by the skimmer [23]. Meanwhile, a full-scale tank consumes large quantities of oil and seawater [7]. In addition, bearing in mind the high sensitivity of oil viscosity to temperature, the variation of ambient conditions along day hours makes the control of experimental precision challenging.

The oleophilic skimming is a special case of the drag-out problem which is the basis of the dip-coating industrial process. The process is still a hot spot for research. The recent areas of study include coating a substrate with a suspension of spherical particles [40], the effect of substrate surface porosity on the entrainment process [42], the characteristics of the liquid sheet ejected by a rotating disc substrate under conditions of high inertia [29], the drag-out of non-Newtonian fluids [43, 46] and deriving formulae to predict the flux of coating liquid on non-flat, e.g. circular, substrate [47]. The drag-out problem has been extensively modelled in the literature in its linear [19, 46] and rotational [37] versions. However, very few, if any, publications considered simulating the multi-fluid oleophilic skimming process.

Whilst, oleophilic skimmers are always considered when handling accidental oil spills, yet their outcome is unpredictable in many circumstances. Besides, the optimum dimensional and operational parameters of the oleophilic skimmer are not well established. Computational simulations under a wide scope of running conditions would particularly fulfil this purpose. The target of this research is to build a reliable computational scheme to simulate the oleophilic skimming process. The rest of this article is organized as follows: Sect. details the numerical method and the case studies, Sect. 3 illustrates the results, discusses the skimming process and compares the findings with the literature, and finally Sect. 4 lists the conclusions of the research and gives recommendations for future work.

## 2 Methods

A two-dimensional model was developed to simulate the process of oil recovery by the drum skimmer. This section details the aspects of the considered geometrical model, numerical technique and ranges of parameters.

### 2.1 Geometry

The geometry of the drum skimmer under investigating is displayed in Fig. 1. The model was designed to emulate realistic site conditions. It comprised a drum that was partially immersed in liquid and rotated clockwise. The drum removed oil from water surface and transferred it to the scraper, over which oil slid till exiting the domain through the right boundary. The scraper was very close to the drum surface to ensure retaining 100% of the skimmed oil. The side walls of the water pool were periodic (cyclic) boundaries, which means the flow crossing one wall re-entered the domain through the other wall. This approaches the actual skimming situation, where the oil moves in the form of surface currents from the drum emerging side to its dipping side where it sticks to the drum surface [23, 31]. In practice, a drum skimmer set involves side brushes to retain the oil that may slip over the drum sides. This was not a concern in the present two-dimensional analysis, since the oil had no opportunity to move in the axial direction. Hence, all the collected oils passed to the scraper and considered in the analysis. Thus, the amount of oil calculated by the simulation approximated that measured in reality.

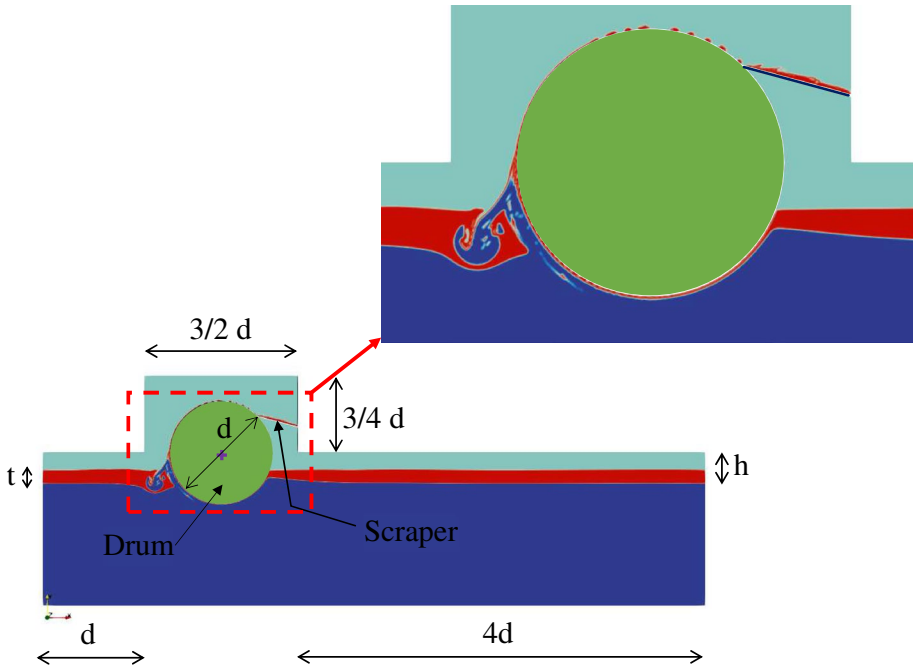


**Fig. 1** The drum skimmer model examined

**Table 1** Properties of oil, water and air at the simulation conditions

| Fluid | Density (kg/m$^3$) | Kinematic viscosity (cSt) | Surface tension (mN/m) |
|---|---|---|---|
| Crude oil | 923 | 99.675 | 31 |
| Seawater | 1026 | 1.189 | 74.08 |
| Air | 1.2257 | 14.657 | |

## 2.2 Fluid properties

The water, slick and atmosphere were assigned the properties of seawater, Endicott crude oil and standard air, respectively. The operating conditions considered were 1.013 bar atmospheric pressure and 15 °C temperature, at which oil properties are easy to obtain from the literature. The hydrodynamic properties of the three fluids are listed in table 1 as excluded from [8, 17, 26]. The oil/water interfacial tension coefficient determines the interfacial force between oil and water. The value considered here was 25.8 mN/m [17].

## 2.3 Mathematical model

The skimming process was simulated by applying the Navier–Stokes Equations to the studied domain considering the three fluids involved, namely oil, water and air. The flow was assumed to be viscous and incompressible [18]. The volume of fluid (VOF) technique was utilised to solve the present multiphase flow problem, since the oil surface was of concern. Unlike the Eulerian model, VOF model analyses all phases using a unique mixture equation for each transport phenomenon. The mixture mass and the momentum conservation equations were defined as

$$\nabla \cdot \vec{V} = 0, \tag{1}$$

$$\rho\left[\frac{\partial \vec{V}}{\partial t} + \left(\vec{V} \cdot \nabla\right)\vec{V}\right] = -\nabla p + \rho\vec{g} + \mu\nabla^2\vec{V} + \vec{f}_{\sigma}, \tag{2}$$

with **V** is the mixture velocity field, $t$ is the time, $p$ is the pressure, $\rho$ is the density, **g** is the gravitational acceleration vector, $\mu$ is the dynamic viscosity, and $\mathbf{f}_{\sigma}$ is the surface tension force. For any pair of immiscible fluids $i-j$, the phase distribution is generated by the interface advection equation, i.e.

$$\frac{\partial \alpha_i}{\partial t} + \vec{V} \cdot \nabla\alpha_i = 0, \tag{3}$$

where $\alpha_i$ is the volume fraction of phase $i$ in a computational cell; $\alpha_i = 1$ means that the cell is entirely occupied with phase $i$, and $\alpha_i = 0$ means the cell is free of phase $i$. For any three phase system, e.g. oil–water–air, $\sum_{i=1}^{3} \alpha_i = 1$. Equation (3) is solved once per phase pair. The mixture properties, $\rho$ and $\mu$, at one cell depend on the phases fractions at that cell, namely

$$\rho = \sum_{i=1}^{3} \alpha_i \rho_i, \tag{4}$$

$$\mu = \sum_{i=1}^{3} \alpha_i \mu_i. \tag{5}$$

The surface tension force is the summation of the interfacial forces between all phase pairs [44], viz.,

$$\vec{f}_{\boldsymbol{\sigma}} = \sigma_{ij}\kappa_{ij}\left(\alpha_j \nabla\alpha_i - \alpha_i \nabla\alpha_j\right), \tag{6}$$

for any $i-j$ phase pair, where $\sigma_{ij}$ is the coefficient of surface tension between the two fluids $i$ and $j$, and $\kappa_{ij}$ is the interface curvature between the two phases. The interface curvature is defined by a pair-averaged gradient of the phase fraction as,

$$\kappa_{ij} = -\nabla \cdot \frac{\alpha_j \nabla\alpha_i - \alpha_i \nabla\alpha_j}{|\,\alpha_j \nabla\alpha_i - \alpha_i \nabla\alpha_j\,|}. \tag{7}$$

## 2.4 Numerical algorithm

The CFD simulations were performed using the open source package OpenFOAM (v19.12). The volume of fluid technique implemented by OpenFOAM is discussed and evaluated in [15]. The multiphaseInterFoam solver was utilised. The pressure–velocity coupling was accomplished by PIMPLE algorithm. For discretisation, the Euler scheme (first order, bounded, implicit) was used for the time derivative ($\partial/\partial t$), the Gauss linear scheme was used for the gradient operator ($\nabla$), the Gauss upwind and Gauss vanLeer schemes were used for the divergence operator ($\nabla\cdot$) and the Gauss linear corrected scheme was used for the Laplacian operator ($\nabla^2$). The time step was dynamic and the Courant number was set not to exceed 0.1 [28] which is a more conservative than typical values [1, 24].

## 2.5 Boundary conditions

In the experimental tests, oil level is kept constant by persistently compensating for the skimmed volume [31]. In the numerical analysis, applying a constant-level boundary condition may cause stability issues [5]. Therefore, some authors tend to extend the domain and add a weir or obstacle followed by a zero-gradient boundary condition [34]. In this research, the domain was extended such that the skimming process could undergo a period of quasi-steady state. This reduced the complexity of the system and imitated the actual situation. The ground of the reservoir as well as the solid parts, i.e. drum and scraper were assigned no-slip conditions. The free top boundaries were assigned a combination of atmospheric-*totalPressure* condition for pressure, zero-*pressureInletOutletVelocity* for velocity and *inletOutlet* for volume fraction. The domain boundaries were named as per Fig. 2 and the conditions applied to each boundary are listed in Table 2.

This research disregarded the effects of waves, currents and winds on the skimming performance, as the focus was on the practical zone of application of the drum skimmer. Oleophilic skimmers are seldom used under severe environmental conditions, where they collect more water than oil. The reader is referred to [2, 3, 11] for examples of oil recovery systems developed to work under rough sea conditions. In the same context, the drum surface material and roughness influence the amount of oil that sticks to the drum [31–33]. The effects of the shape, pattern and mean height of the roughness elements are far beyond the scope of the present analyses.

**Table 2** Summary of the conditions set at the problem boundaries

| Boundary | $U$ | $p-\rho gh$ | $\alpha_{\text{air}}$ | $\alpha_{\text{water}}$ | $\alpha_{\text{oil}}$ |
|---|---|---|---|---|---|
| Inlet | Cyclic | | | | |
| Outlet | Cyclic | | | | |
| Bed | [0 0 0] | $\partial/\partial n^{\dagger}=0$ | $\theta^{*}=90°$ | $\partial/\partial n=0$ | |
| Atmosphere | $\partial/\partial n=0$ | $p=0$ | $\partial/\partial n=0$ | $\alpha=0$ | |
| Drum | $\omega^{\ddagger}$ | $\partial/\partial n=0$ | $\theta$=90° | $\partial/\partial n=0$ | |
| Scraper | [0 0 0] | $\partial/\partial n=0$ | $\theta$=90° | $\partial/\partial n=0$ | |

† Boundary-normal direction

* Contact angle

‡ The linear velocity vector was calculated from the drum rotational speed

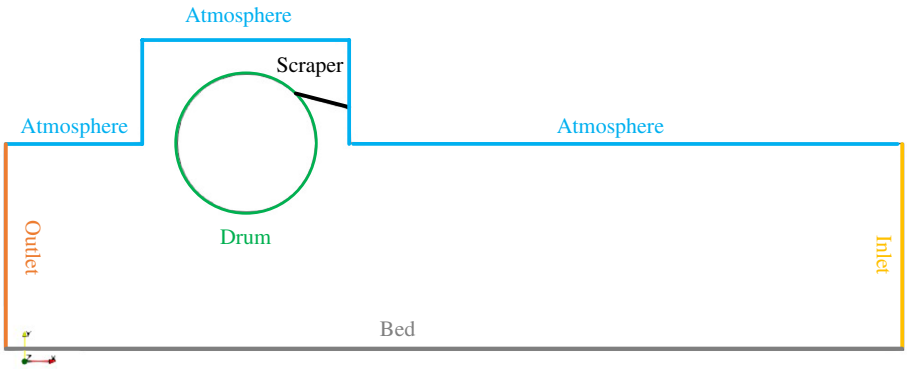


**Fig. 2** Defining the problem boundaries

From the literature [23, 31] and from practical observations, the currents of the oil on water surface in the skimming process can be illustrated by Fig. 3. In the preliminary tests of the current study, not shown here, the author investigated the effect of the boundary condition on the simulation of the skimming process. Applying the no-slip condition to the side boundaries ended up with the oil piling at the emerging side of the drum and washing the collected oil layer off the drum surface, which led to reducing the modelled oil recovery rate.

### 2.6 Mesh

The basic mesh was built using the *blockMesh* tool of the OpenFOAM. Square 1×1 mm cells were utilised. Then the solid parts, i.e. drum and scraper were inserted via the *snappyHexMesh* tool. The *snappyHexMesh* tool was used for cutting the background mesh, snipping the neighbour cells to the solid surfaces and refining the near-wall regions. The final mesh was too fine to illustrate, but its quality can be perceived from the fine oil drops captured by the grid in Figs. 1 and 4 due to the large number of cells simulating each drop.

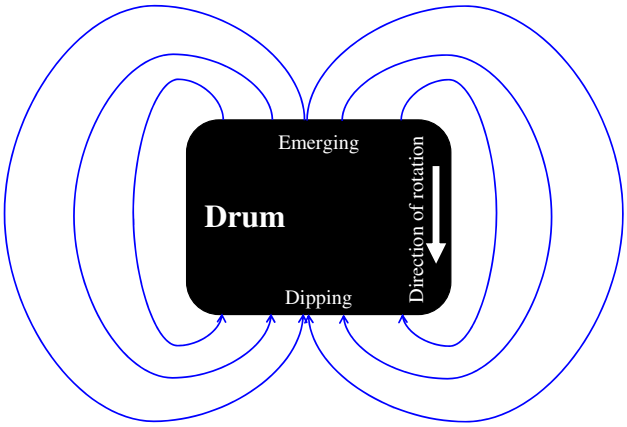


**Fig. 3** Currents of the oil on the water surface in a skimming process

### 2.7 Test cases

The numerical experiment was designed to involve all (seven) variables affecting the oil recovery rate according to the literature. Each parameter was assigned at least four values covering its practical range, with the other parameters fixed at their base (default) values. The parameters investigated and their values are listed in Table 3. The drum diameter was varied by scaling up/down the flow domain, utilising the OpenFOAM function *transformPoints*, whilst keeping the drum centre height and oil slick thickness at their base values. A total of 34 simulation cases were involved.

## 3 Results and discussion

### 3.1 Model validation

Before proceeding with the simulations, it was a must to confirm the independence of the results from the numerical

**Table 3** Values of the parameters tested

| Parameter | Values [base value] |
|---|---|
| Oil kinematic viscosity ($\nu$, cSt) | 1, 10, 50, [100], 500, 1000 |
| Oil density ($\rho$, kg/m$^3$) | 750, 825, [923], 975 |
| Oil surface tension ($\sigma$, mN/m) * | 20, 24, 27, [31] |
| Drum rotational speed ($N$, rpm) | 15, 30, 45, [60], 75 |
| Drum diameter ($d$, mm) | 150, 200, 250, [300], 350, 400 |
| Drum centre height ($h$, mm) | 30, 60, [90], 120 |
| Oil slick thickness ($t$, mm) | 5, 10, 15, [25], 40 |

* Oil/seawater interfacial tension was calculated from Girifalco and Good equation [35] assuming an interfacial interaction parameter $\phi$ of 0.83

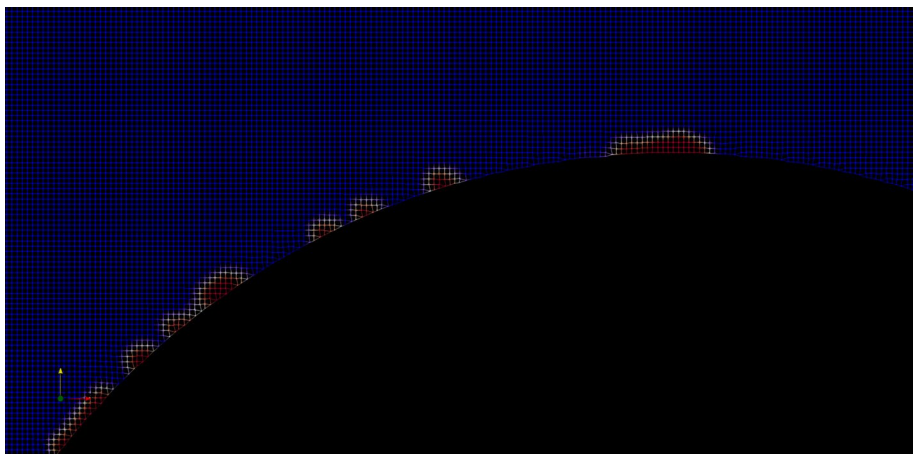

**Fig. 4** A close-up view of the mesh near the drum surface

model applied. Solution convergence was assured per grid resolution, time step and domain size. Five grids were examined in the mesh-dependency analysis. The meshes were termed M8, M9, M10, M11 and M12 and comprised 8, 9, 10, 11 and 12 square cells per cm length. The comparison was based on the change of the total oil volume with time, assuming a one-metre length drum. This volume was calculated by applying the *Integrate Variables* filter of ParaView to determine the volume-integral of fluid fraction throughout the domain. The results of the five meshes are given in Fig. 5. The figure approves the grid-independence of meshes finer than M9, which validates the current 10 cells/cm mesh.

Comparison of the total number of grid cells and relative execution time of the meshes under investigation are given in Fig. 6. Mesh M10 was assigned a 100-unit time, and the execution time of the other meshes was computed accordingly.

The time step, expressed by the Courant number, is very crucial in multi-phase transient flow analysis. Five values of Courant number were tested herein: $C = 1.0$, $C = 0.5$, $C = 0.25$, $C = 0.125$ and $C = 0.0625$. The variation of the domain oil volume with time for the cases is illustrated in Fig. 7. The solution converged at Courant number $C = 0.125$ which ensures the fidelity of the time step assigned in the present research, $C = 0.1$ [28].

A third check was conducted on convergence with domain size. Three domain extensions were explored in this context: 2d, 4d and 6d, resembling domain lengths of 75 + 60, 75 + 120 and 75 + 180 cm. Note that the entire length is free of boundaries since the domain is cyclic. The adequate parameter for comparison between these cases of different volumes was the cumulative oil recovery rate (ORR, LPM) per unit length of the drum. The results are plotted in Fig. 8. The figure displays also the water ingestion rate (WIR), which is an indicator of the skimmer efficiency. As demonstrated by Fig. 8, ORR and WIR witnessed a period

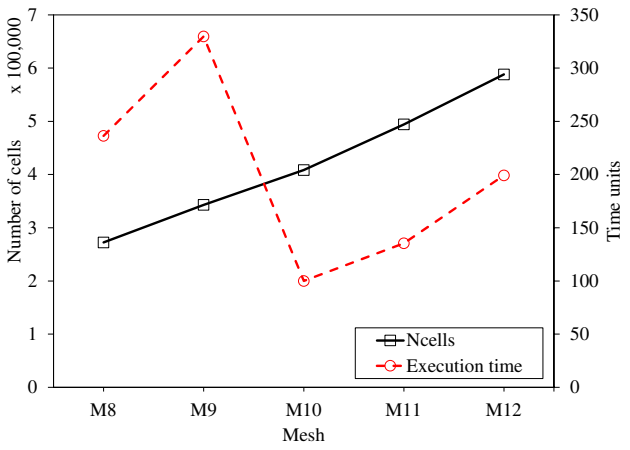


**Fig. 6** The number of cells and relative execution time of the inspected mesh sizes

of quasi-steady state. In the present analysis, the skimmer ORR was denoted by the maximum ORR during the quasi-steady period. The value of WIR at the corresponding time was considered for further analysis. According to this definition, the 2d, 4d and 6d domains yielded ORRs of 63.8, 65.0 and 66.0 LPM and WIRs of 7.31, 6.89 and 6.8 LPM. It was decided that a 4d-extension was appropriate for the rest of the simulations. Figure 9 gives consecutive snapshots from the skimming process. The next subsections discuss the effect of the operational variables on the drum skimmer performance.

## 3.2 Rotational speed

The skimmer performance varies with drum rotational speed as per Fig. 10. The amount of oil recovered per minute was proportional to the number of drum revolutions. The same was true for the amount of water ingested. Beyond 45 rpm,

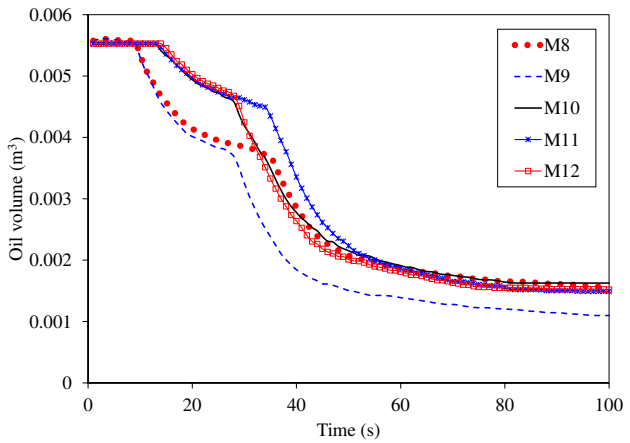


**Fig. 5** Total oil volume change with time of the five studied meshes

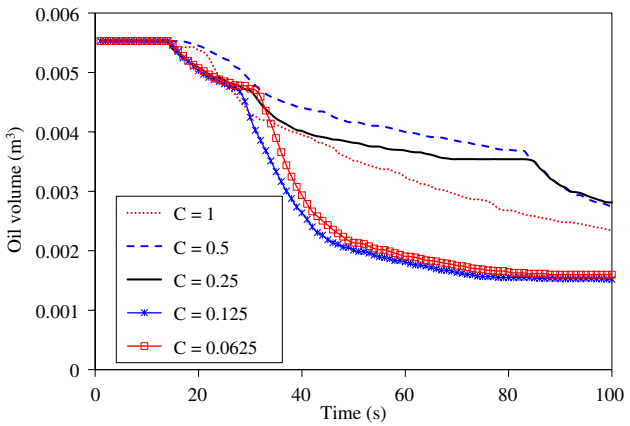


**Fig. 7** Total oil volume change with time of the five Courant numbers

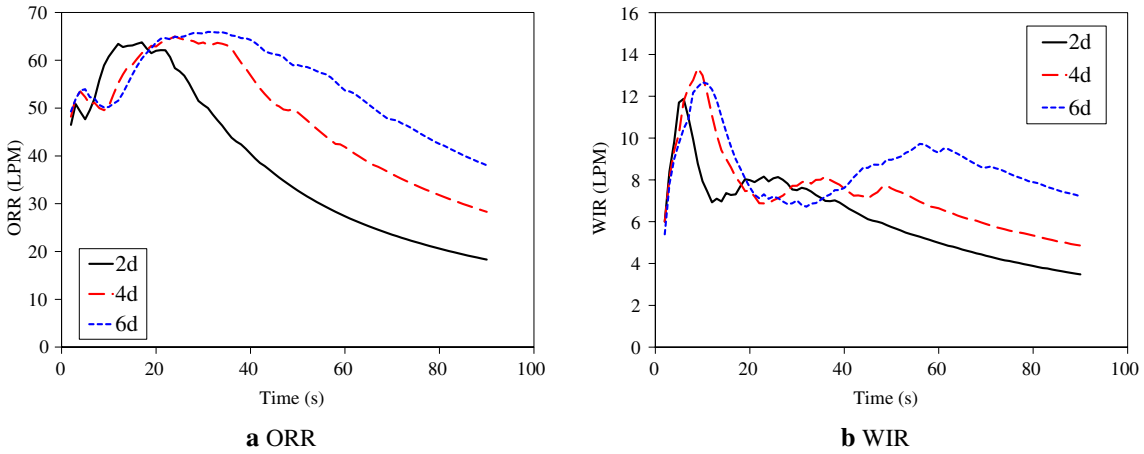


**a** ORR **b** WIR

**Fig. 8** Domain size check; cumulative oil recovery and water ingestion rates versus time

WIR witnessed a drastic increase, which led to a decline in value and rate of increase of ORR with rotational speed. Thence, running the drum at higher speeds is less effective.

### 3.3 Fluid properties

The effects of oil properties, namely, viscosity, density and surface tension are displayed in Figs. 11–13, respectively. The viscosity determines the ability of oil to stick to the drum surface, as well as water. Thin oils ($\nu < 10$ cSt) could hardly stick to the drum surface, whereby heavy oils ($\nu > 100$ cSt) absorbed substantial amounts of water. It is recommended to employ oleophilic skimmers exclusively within the range of oil viscosities of 10 to 100 cSt. Besides, ORR reached a saturation state at high viscosities ($\nu > 100$ cSt).

Oil density measures the weight of the oil slick and the buoyant force acting on it by water. As indicated in Fig. 12, ORR declined when skimming denser oils. This was not only because it was harder for the drum to carry heavier oils. Other reasons were: 1) the increase of the amount of the skimmed water, since its weight became comparable to that of oil and 2) the loss of more oil to the pool in the submergence period, because it got subjected to a weaker buoyant force.

Neither oil surface tension nor oil/water interfacial tension affects ORR or WIR of the skimmer in the examined ranges, as shown in Fig. 13. The capillary number ($U\mu/\sigma$) in this analysis varied between 2.8 and 4.3, which is quite larger than unity. The skimming process is, consequently, dominated by drum traction (inertia force), gravitational force and viscous force. The classical drag-out problem suggests the oil flow rate to reach an asymptotic value under these conditions [29, 30]. This result contradicts with the findings of Hammoud and Khalil [23]. Most likely, this evolved in their experimental investigations from the tangled relationship between the surface tension and the other oil properties; neither could be changed separately. This is a power point of the present simulation.

### 3.4 Geometry

By geometry, the author means the drum diameter, drum centre height and oil slick thickness. These parameters influence the skimmer performance according to Figs. 14–16, respectively. Linearity dominated the correlation between ORR and drum diameter (Fig. 14). The analogy with the ORR–rotational speed ($N$) relationship (Fig. 10) is evident since both parameters influence the viscous shear velocity ($\pi dN/60$) through a direct proportion. On the other hand, WIR increased exponentially with drum diameter. The amount of ingested water exacerbated with drum diameters larger than 300 mm.

The impact of the drum centre height is complicated. As the drum centre went further from the oil/water interface, the oil submergence period became shorter. Hence, less of the skimmed oil fell back to the pool, and less water was ingested. On the other hand, the oil journey from the pool to the scraper became longer. The resulting skimmer performance (Fig. 15) reflects a fluctuation in ORR and WIR with centre height. According to the figure, it is suggested to operate the skimmer at centre height ratios ($h/d$) between 0.3 and 0.4 to accomplish high ORR with low WIR.

With regard to oil slick thickness (Fig. 16), ORR improves and WIR declines by thickening the oil slick throughout the studied range. Increasing oil slick thickness by booming is very efficient in WIR reduction. According to Fig. 16, the performance of the drum skimmer extremely degrades when the slick thickness falls below 25 mm.

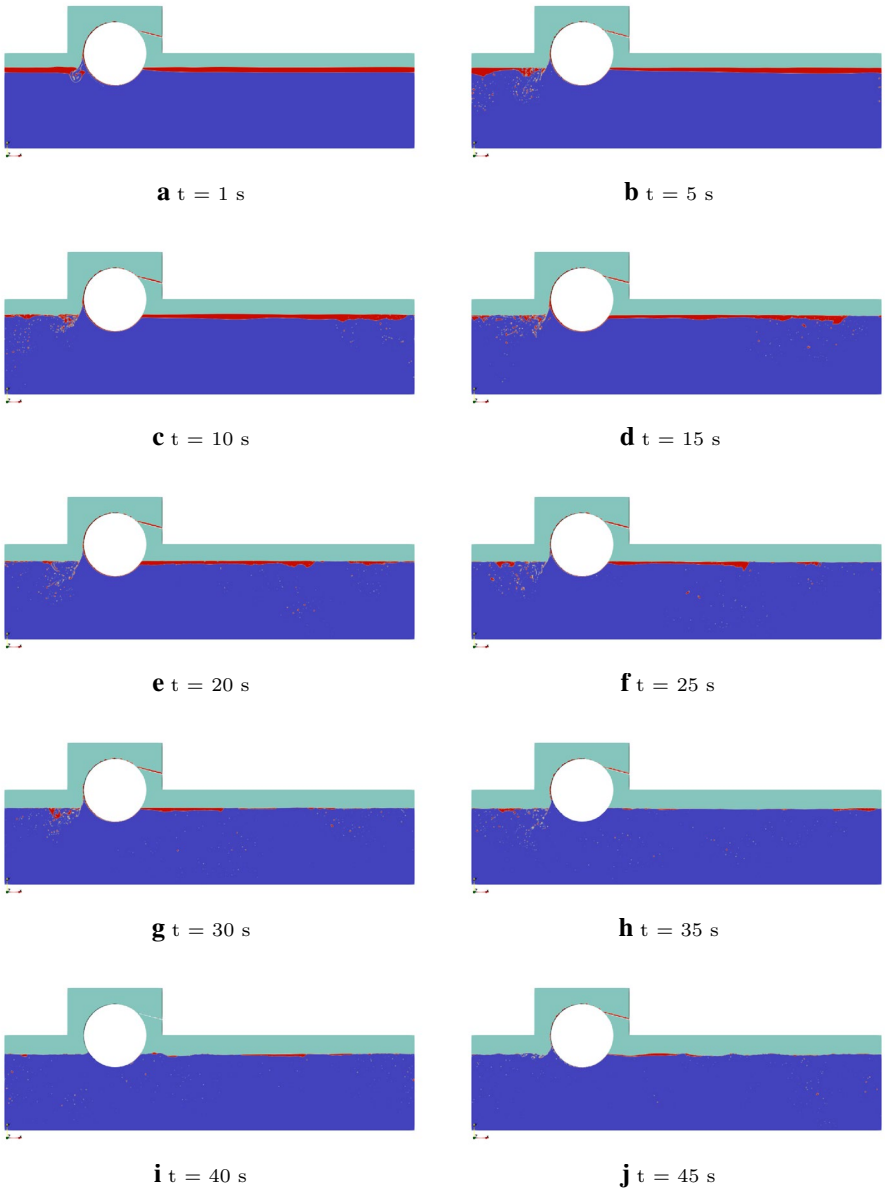


**Fig. 9** Snapshots from the skimming process

### 3.5 Non-dimensional analysis

The problem can be reformulated in a dimensionless form. The drum rotational speed, geometry and fluid properties were expressed in terms of dimensionless oil recovery rate ($q_o = \mathrm{ORR}/\omega d^2$), dimensionless water ingestion rate ($q_w = \mathrm{WIR}/\omega d^2$), Reynolds number ($Re = \omega d^2/\nu$), Webber number ($We = \rho\omega^2 d^3/\sigma$), dimensionless centre height ($H = h/d$) and dimensionless thickness ($T = t/d$). The effect of the dimensionless parameters is illustrated in Fig. 17. Notably, the dimensionless oil and water gathering rates settle to constant values at high Webber numbers, i.e. high inertia to surface tension force ratio.

### 3.6 Validation of the results

The results of the present analysis were validated with the well-established experimental data of Broje and Keller [8], see Fig. 18. The data reported by Broje and Keller were acquired with a slightly larger drum ($d = 356$ mm), under a higher ambient temperature (25 °C) and with two oils (Endicott, $\rho = 907$ kg/m$^3$ and $\nu = 55$ cSt; HydroCal 300, $\rho = 905$ kg/m$^3$ and $\nu = 179$ cSt). Linear interpolations were applied to account for the differences in the operating conditions between the experimental and numerical sets of data. The trends and values are in good agreement, which confirm the reliability of the CFD results. The numerical simulation

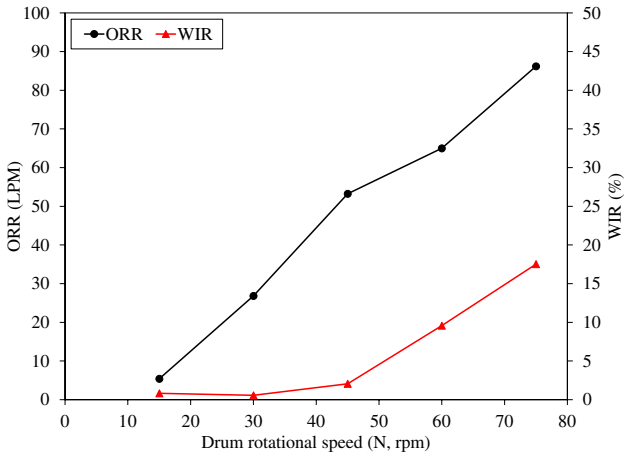


**Fig. 10** Variation of ORR and WIR with drum rotational speed

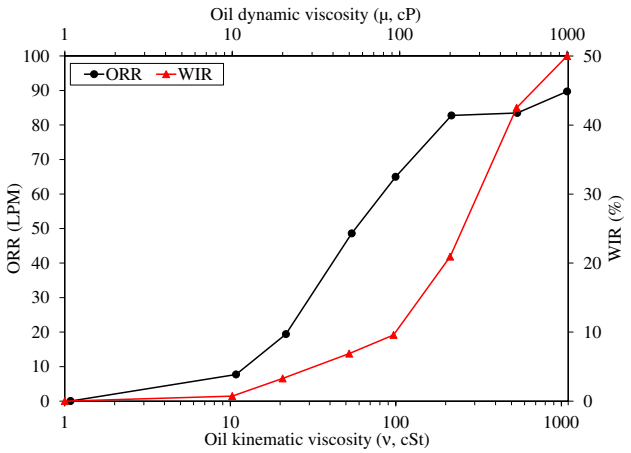


**Fig. 11** Variation of ORR and WIR with oil viscosity

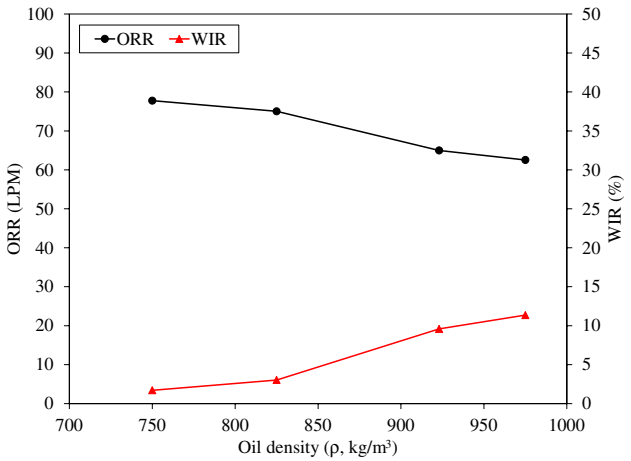


**Fig. 12** Variation of ORR and WIR with oil density

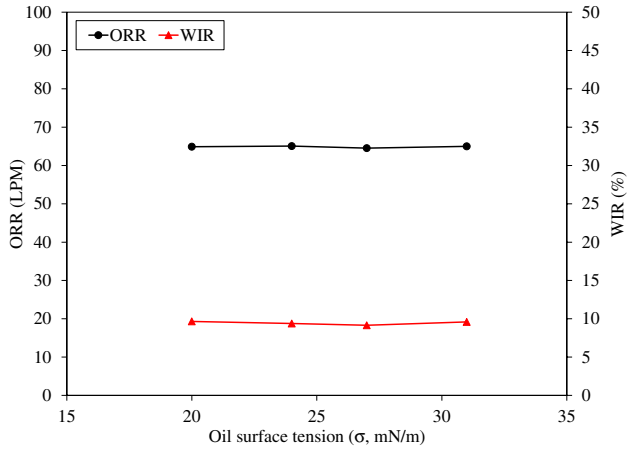


**Fig. 13** Variation of ORR and WIR with oil surface tension

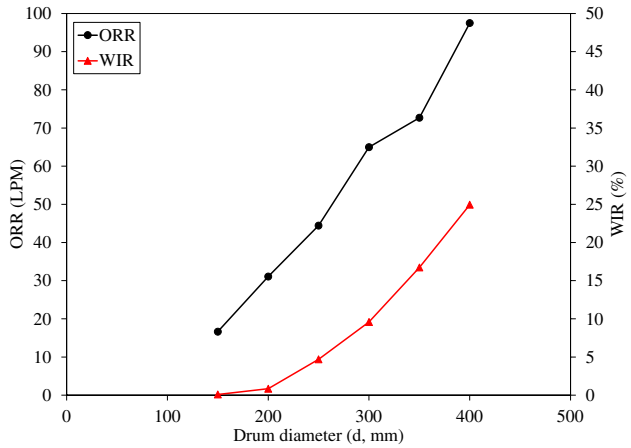


**Fig. 14** Variation of ORR and WIR with drum diameter

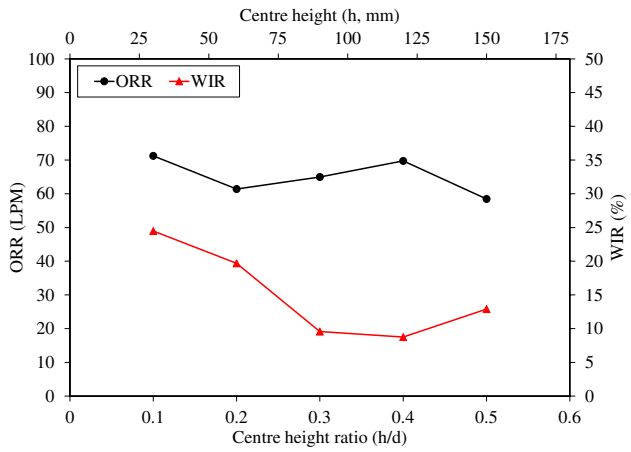


**Fig. 15** Variation of ORR and WIR with drum centre height

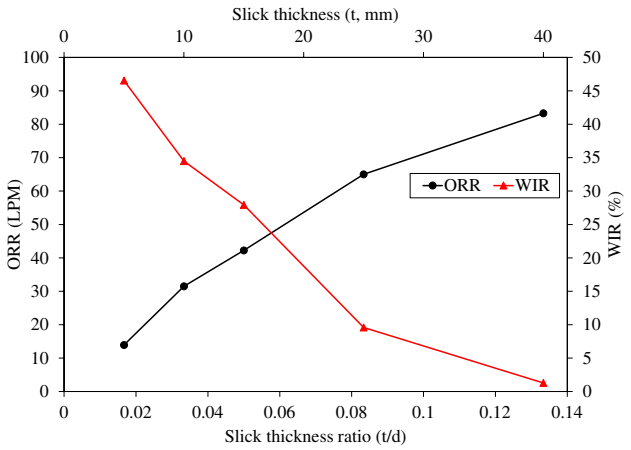


**Fig. 16** Variation of ORR and WIR with oil slick thickness

assumed a perfect scraping process, which led to its results slightly exceeding the experimental values, specially at high speeds.

## 4 Conclusions

The oleophilic skimming, in spite of its wide use in oil spill recovery, has no reliable general formulation of its performance. The existing experimental literature lacks generality and accuracy. The current research aimed to develop a numerical methodology to model oil skimming by a drum. The operational conditions were changed to cover the practical ranges of implementation. The results gave a thorough insight into the influence of each operating parameter on the drum performance. This can accurately guide the manufacturing and operating processes. In addition, the following conclusions were drawn:

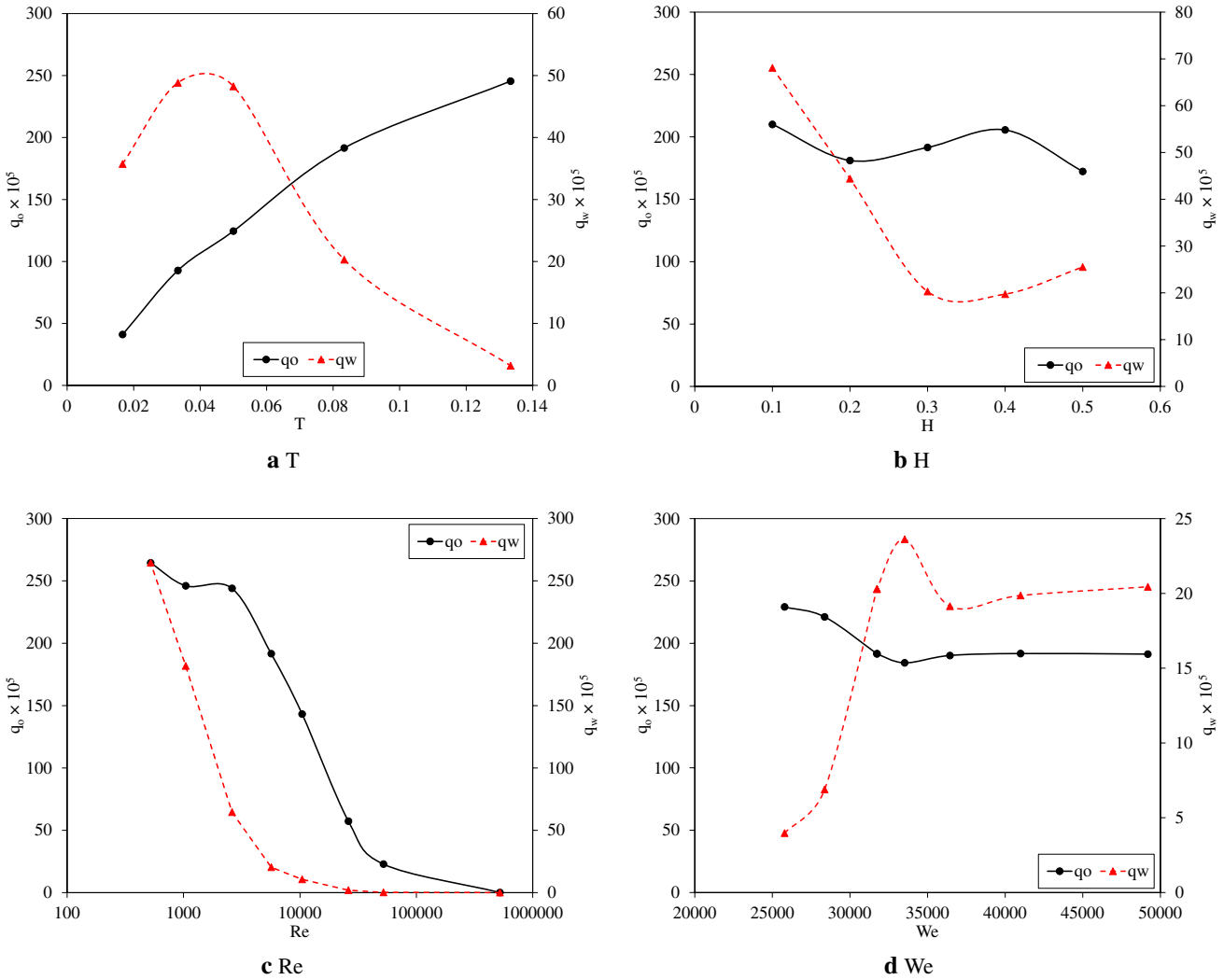


**a** T **b** H **c** Re **d** We

**Fig. 17** Variation of the dimensionless ORR and WIR with the different parameters

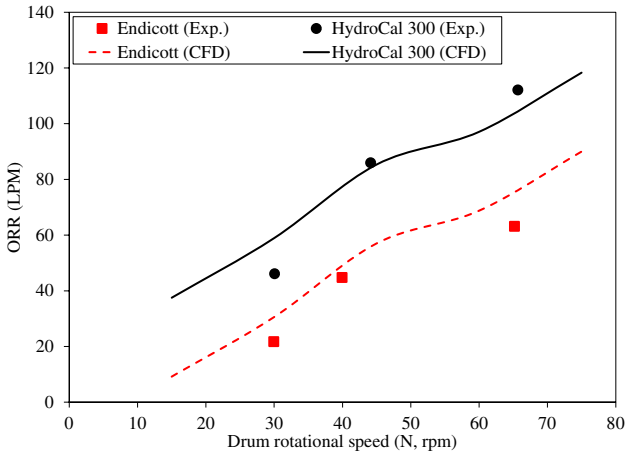


**Fig. 18** Validation of the simulation results (CFD) with data from the literature (Exp.)

- The oil recovery rate varies linearly with rotational speed and drum diameter. The percentage of ingested water ratio increases tremendously (> 10 %) at rotational speeds higher than 45 rpm and drum diameters larger than 300 mm.
- The drum delivers its maximum amount of oil at drum centre height ratios of 0.1 and 0.4, with the latter ingesting the minimum amount of water.
- The oil slick thickness is recommended not to be less than 25 mm to ensure a high rate of oil recovery and a limited amount of ingested water.
- The drum skimmer performs best when collecting oils of viscosities between 10 and 100 cSt. Heavier oils gather excessive amounts of water, whereas lighter oils do not stick to the drum.
- The increase in oil density drives a slight decline in ORR due to the increase in gravitational force. By contrary, WIR increases as the density of oil approaches that of water.
- Oil surface tension, in the studied range, does not alter ORR or WIR.

One important feature of the aforementioned conclusions is their applicability to the other types of oleophilic skimmers and dip-coating processes. Further research is needed to predict the impact of sea disturbance on the drum skimmer performance and how to improve the performance through surface modifications.

**Acknowledgements** This work was supported by computational resources provided by the Bibliotheca Alexandrina on its High-Performance Computing (HPC) infrastructure (hpc.bibalex.org).

**Funding** Open access funding provided by The Science, Technology & Innovation Funding Authority (STDF) in cooperation with The Egyptian Knowledge Bank (EKB).

## Declarations

**Conflict of interest** The author certifies that he has NO affiliations with or involvement in any organization or entity with any financial interest or non-financial interest in the subject matter or materials discussed in this manuscript.



## References

1. Abbassi W, Besbes S, El Hajem M et al (2017) Influence of operating conditions and liquid phase viscosity with volume of fluid method on bubble formation process. Eur J Mech B Fluids 65:284–298
2. Abu Amro M, Sprenger F, Berlin T (2008) An innovative offshore oil skimming system for operations in harsh seas. Ship Technol Res 55(4):147–156
3. Agrusta A, Filippo B, Luigi P, et al (2013) Oil skimmers for coastal waters and open sea cleaning. In: 16th International Conference on Transport Science, Narodna in univerzitetna knjiznica, pp 1–11
4. Algawai RJ, Dawood MA (2017) Study of operating conditions for oil skimmer apparatus from water. In: ResearchGate Conference paper-322303173
5. Bayon-Barrachina A, Lopez-Jimenez PA (2015) Numerical analysis of hydraulic jumps using openfoam. J Hydroinform 17(4):662–678
6. Belore RC, Trudel K, Mullin JV et al (2009) Large-scale cold water dispersant effectiveness experiments with alaskan crude oils and corexit 9500 and 9527 dispersants. Mar Pollut Bull 58(1):118–128
7. Broje V, Keller AA (2006) Improved mechanical oil spill recovery using an optimized geometry for the skimmer surface. Environm Scie Technol 40(24):7914–7918
8. Broje V, Keller AA (2007) Effect of operational parameters on the recovery rate of an oleophilic drum skimmer. J Hazard Mater 148(1–2):136–143
9. Chenhao J, Yupeng X (2021) Risk analysis and emergency response to marine oil spill environmental pollution. In: IOP Conference Series: Earth and Environmental Science, IOP Publishing, p 012070
10. Clauss G, Amro MA (2004) Two and three-phase flow computation for the optimization of oil skimming systems. In: 3rd International Symposium on two-phase flow modeling and experimentation, Pisa
11. Clauss G, Habel R, Vannahme M, et al (2002) Development of oil skimming vessels for high seas. In: 10th International Congress

of the International Maritime Association of the Mediterranean, IMAM-2002, Crete, Greece
12. Clauss G, Abu-Amro M, Kosleck S (2006a) Numerical and experimental optimization of a seaway independent oil skimming system-sos. In: The Sixteenth International Offshore and Polar Engineering Conference, OnePetro
13. Clauss G, Kosleck S, Abu-Amro M, et al (2006b) Computational fluid dynamics for the simulation of oil recovery systems at high seas. In: Proceedings of the 25th International Conference on Offshore Mechanics and Arctic Engineering
14. Commission MM et al (2011) Assessing the long-term effects of the bp deepwater horizon oil spill on marine mammals in the gulf of mexico: a statement of research needs. Marine Mammal Commission, Bethesda, Maryland
15. Deshpande SS, Anumolu L, Trujillo MF (2012) Evaluating the performance of the two-phase flow solver interfoam. Comput Sci Discov 5(1):014016
16. El-Gayar D, Khodary M, Abdel-Aziz M et al (2021) Effect of disk skimmer material and oil viscosity on oil spill recovery. Water Air Soil Poll 232(5):1–9
17. Environmental Science and Technology Centre (2014) Environment Canada crude oil and petroleum product database. Data retrieved from Environment Canada, https://etc-cte.ec.gc.ca/databases/OilProperties
18. Feng X, Li Y (2018) Numerical simulation of the flow channel in the curved plane oil skimmer. Int J Mar Sci 11(11):1842–1846
19. Filali A, Khezzar L, Mitsoulis E (2013) Some experiences with the numerical simulation of newtonian and bingham fluids in dip coating. Comput Fluids 82:110–121
20. Filippov A, Ishmuratov T (2013) Hydrodynamics of the fluid layer on the drum of an adhesion skimmer. J Appl Mech Tech Phys 54(5):781–788
21. Godawarikar S, Gavhane A (2020) Literature review on oil recovering skimmer from the surface of water. Int J Eng Res Technol 7:3956
22. Griggs JW (2011) Bp gulf of mexico oil spill. Energy LJ 32:57
23. Hammoud A, Khalil M (2003) Performance of a rotating drum skimmer in oil spill recovery. Proc Inst Mech Eng 217(1):49–57
24. Heinrich M, Schwarze R (2020) 3d-coupling of volume-of-fluid and lagrangian particle tracking for spray atomization simulation in openfoam. SoftwareX 11(100):483
25. Hoang AT, Pham VV, Nguyen DN (2018) A report of oil spill recovery technologies. Int J Appl Eng Res 13(7):4915–4928
26. Hollebone BP (2014) Appendix a the oil properties data appendix. Handbook of oil spill science and technology pp 575–681
27. ITOPF (2021) Oil tanker spill statistics 2021. Data retrieved from International Tanker Owners Pollution Federation Limited, https://www.itopf.org/
28. Jamshidi F, Heimel H, Hasert M et al (2019) On suitability of phase-field and algebraic volume-of-fluid openfoam® solvers for gas-liquid microfluidic applications. Comput Phys Commun 236:72–85
29. Jerome JJS, Thevenin S, Bourgoin M, et al (2021) Inertial drag-out problem: sheets and films on a rotating disc. Journal of Fluid Mechanics 908
30. Jin B, Acrivos A, Münch A (2005) The drag-out problem in film coating. Phys Fluids 17(10):103603
31. Khalil M, El-Boghdady I, Lotfy E (2021a) Enhancement of drum skimmer oil-spill recovery performance by using nano-ceramics coating under different operating conditions. Design Engineering pp 710–721
32. Khalil M, El-Boghdady I, Lotfy E (2022) Oil-recovery performance of a sponge-covered drum skimmer. Alex Eng J 61(12):12653–12660
33. Khalil MF, Elmaradny AA, Lotfy ER (2021b) Experimental investigation of the effect of prismatic roughness on the performance of belt skimmers in oil spill recovery applications. In: 2021 6th International Conference on Mechanical Engineering and Robotics Research (ICMERR), IEEE, pp 66–71
34. Lewandowski H, Meinikmann K, Krause S (2020) Groundwater-Surface Water Interactions. MDPI AG
35. Makkonen L, Kurkela J (2018) Another look at the interfacial interaction parameter. J Colloid Interface Sci 529:243–246
36. McKinney K, Caplis J, DeVitis D, et al (2017) Evaluation of oleophilic skimmer performance in diminishing oil slick thicknesses. In: International Oil Spill Conference Proceedings, International Oil Spill Conference, pp 1366–1381
37. Miah MS, Al-Assaf S, Yang X et al (2016) Thin film flow on a vertically rotating disc of finite thickness partially immersed in a highly viscous liquid. Chem Eng Sci 143:226–239
38. Nam C, Li H, Zhang G et al (2018) Practical oil spill recovery by a combination of polyolefin absorbent and mechanical skimmer. ACS Sustain Chem Eng 6(9):12036–12045
39. Ni S, Qiu W, Zhang A et al (2015) Hydrodynamic simulation and optimization of an oil skimmer. J Offshore Mech Arct Eng 137(2):021301
40. Palma S, Lhuissier H (2019) Dip-coating with a particulate suspension. J Fluid Mech 869:R3
41. Sabbar W, Mohammed B, Almudhaffar M (2021) Influence of operational parameters on the recovery rate of polyester resin surface of locally designed drum oil skimmer. In: Journal of Physics: Conference Series, IOP Publishing, p 012023
42. Sathyanath R, Aarthi A, Kalpathy SK (2020) Liquid film entrainment during dip coating on a saturated porous substrate. Chem Eng Sci 218(115):552
43. Smit WJ, Kusina C, Colin A et al (2021) Withdrawal and dip coating of an object from a yield-stress reservoir. Phys Rev Fluids 6(6):063302
44. Vakhrushev A, Wu M, Ludwig A, et al (2014) Experimental verification of a 3-phase continuous casting simulation using a w ater model. In: Proceedings 8th ECCC Conference, Graz
45. Wang Y, Liu X, Yu X et al (2018) Assessing response capabilities for responding to ship-related oil spills in the chinese bohai sea. Int J Disaster Risk Reduct 28:251–257
46. Zhang HK, Yin YR, Zhang XM et al (2021) Numerical simulation of the hydrodynamics of yield stress fluids during dip coating. J Nonnewton Fluid Mech 298(104):675
47. Zhang Z, Salamatin A, Peng F et al (2022) Dip coating of cylinders with newtonian fluids. J Colloid Interface Sci 607:502–513